Comparison of two vascular-disrupting agents at a clinically relevant dose in rodent liver tumors with multiparametric magnetic resonance imaging biomarkers

Huaijun Wang[a], Marlein Miranda Cona[a], Feng Chen[a,b], Jie Yu[a], Yuanbo Feng[a], Junjie Li[a], Frederik De Keyzer[a], Guy Marchal[a] and Yicheng Ni[a]

We sought to compare the therapeutic efficacy between two vascular-disrupting agents, combretastatin A4 phosphate (CA4P) and ZD6126, at a clinically relevant dose on tumor models with magnetic resonance imaging (MRI). Thirty rats with liver rhabdomyosarcoma were randomized into CA4P (10 mg/kg), ZD6126 (10 mg/kg), and control group ($n=10$ for each group). Multiparametric MRI biomarkers including tumor volume, enhancement ratio, necrosis ratio, apparent diffusion coefficient (ADC), and K^{trans} (volume transfer constant) derived from T2-weighted, T1-weighted, contrast-enhanced T1-weighted, and diffusion-weighted imaging, and dynamic contrast-enhanced MRI were compared at pretreatment, 1 h, 6 h, 24 h, 48 h, and 120 h posttreatment; they were validated using ex-vivo techniques. Relative to rapidly growing tumors without necrosis in control rats, tumors grew slower in the CA4P group compared with the ZD6126 group with a higher necrosis ratio at 120 h ($P<0.05$), as proven by histopathology. In the CA4P group, K^{trans} decreased from 1 h until 6 h, and partially recovered at 120 h. In the ZD6126 group, the reduced K^{trans} at 1 h began to rebound from 6 h and exceeded the baseline value at 120 h ($P<0.05$), parallel to evolving enhancement ratios ($P<0.05$). ADC revealed more necrotic tumors with CA4P versus ZD6126 at 120 h ($P<0.05$). The different tumor responses were confirmed by ex-vivo microangiography and histopathology. CA4P was more effective than ZD6126 in impairing blood supply, inducing necrosis, and delaying growth in rat liver tumors at a clinically relevant dose. A single dose of vascular-disrupting agent was insufficient to destroy the tumor. The multiparametric MRI biomarkers enabled in-vivo noninvasive comparison of therapeutic efficacy between CA4P and ZD6126. *Anti-Cancer Drugs* 23:12–21 © 2011 Wolters Kluwer Health | Lippincott Williams & Wilkins.

Anti-Cancer Drugs 2012, **23**:12–21

Keywords: combretastatin A4 phosphate, imaging biomarkers, magnetic resonance imaging, microangiography, tumor, vascular-disrupting agent, ZD6126

[a]Department of Radiology, University Hospitals, University of Leuven, Belgium and [b]Department of Radiology, Zhongda Hospital, Southeast University, Nanjing, China

Correspondence to Yicheng Ni, Department of Radiology, University Hospitals, University of Leuven Herestraat 49, Leuven B-3000, Belgium
Tel: +32 16 330165; fax: +32 16 343765;
e-mail: Yicheng.Ni@med.kuleuven.be

Received 31 January 2011 **Revised form accepted** 14 June 2011

Introduction

Solid malignancies have to develop their own functional vasculature for metabolic demands to maintain survival and aggressive growth when their diameter exceeds a few millimeters [1]. The newly formed tumor vessels are immature in both structure and functionality compared with normal vessels. Consequently, the tumor vasculature becomes an actual target for therapy because of its crucial role in nutrition or oxygen supply and access of blood-borne antitumor drugs to the tumor [2]. Possible approaches include inhibition of neoangiogenesis and destruction of existing tumor vessels. The latter refers to vascular-disrupting therapy that, by exploiting the differences between normal and tumor vessels, selectively causes vascular shutdown in the tumor, leading to secondary ischemic tumor cell death or necrosis [3].

Among vascular-disrupting agents (VDAs), zybrestat [combretastatin A4 phosphate (CA4P)] and ZD6126 target microtubules of vascular endothelial cytoskeleton. CA4P is the water-soluble prodrug of combretastatin A4, which was first isolated from the African bush willow tree *Combretum caffrum* [4]; ZD6126 is a derivative of colchicine, which is rapidly converted *in vivo* into ZD6126 phenol (*N*-acetyl-colchinol) [5]. They both selectively bind to the tubulin of cytoskeleton and cause its depolymerization, leading to contraction (rounding up) of the endothelial cells lining the tumor blood vessels, vascular hyperpermeability, decreased blood flow, and resultant tumor necrosis [6]. However, they cannot actively eradicate tumors, and can only delay the tumor growth.

Both CA4P and ZD6126 have a wide therapeutic window below maximum-tolerated dose (MTD) in animals, and their tumoricidal effects can be exerted well below the MTD [2,7,8]. However, high doses of VDAs have often been experimentally used in tumor models to achieve significant antitumor effects. However, such promising outcomes cannot be easily translated into clinical patients, because the high doses often exceed the MTD in humans. Therefore, the vascular shutdown

0959-4973 © 2011 Wolters Kluwer Health | Lippincott Williams & Wilkins DOI: 10.1097/CAD.0b013e328349dd60

effect with a clinically relevant dose in tumor models may yield results more predictable to patients in bench-to-bedside research. According to preclinical and clinical data, CA4P at a dose of 10 mg/kg in rats gives a plasma exposure equivalent to that achieved with the MTD of 65 mg/m^2 dose in humans [9]; ZD6126 at a dose of 10 mg/kg in rats is equivalent to the MTD of 112 mg/m^2 dose in humans [10].

Given the novel mechanism of action with VDAs, classical endpoints of tumor response and tumor regression need to be revised. Development of quantitative imaging biomarkers has led to an increased use of imaging in the assessment of tumor vasculature. Thus, there is a need to better understand how imaging biomarkers may contribute to the evaluation of therapeutic events, including early hemodynamic changes in vascular beds and tumor growth endpoint. Magnetic resonance imaging (MRI) has been the most commonly used modality due to its intrinsic capacity and flexibility to provide a wide range of pathophysiological information, especially by using diffusion-weighted imaging (DWI) and dynamic contrast-enhanced MRI (DCE-MRI).

Although CA4P and ZD6126 have both shown vascular shutdown effects in preclinical research and clinical trials, the comparison of therapeutic efficacy between CA4P and ZD6126 at a clinically relevant dose has never been performed in tumor models on a clinical MRI scanner with multiple imaging biomarkers. To our knowledge, there is only one report comparing their different treatment outcomes with MR spectroscopy at a 7.0 T scanner [11]. Therefore, we conducted this study to directly compare therapeutic effects of these two lead VDAs: a well-established rat liver tumor model was used to mimic oncologic patients; a clinically relevant dose of either VDA was intravenously administered to treat the tumors; multiparametric MRI biomarkers were acquired at clinical 1.5 T MRI; and the derived imaging biomarkers were compared and verified with postmortem micro-angiography and histopathology. Thus, the two VDAs in a novel anticancer therapy based on drug-induced micro-vascular intervention have been studied mainly by using advanced imaging technology.

Materials and methods

Tumor model

This study was approved by the local Ethics Committee for Animal Care and Use. The rhabdomyosarcoma (R1) tumor cell line with highly reproducible biological features and stable responses to treatments was maintained by passages with the syngeneic subcutaneous transplantation [12,13].

Male WAG/Rij rats aged approximately 14 weeks old, weighing 220 – 270 g, received the intrahepatic tumor implantation in the liver. In brief, rats were anesthetized with intraperitoneal pentobarbital (Nembutal; Sanofi Sante Animale, Brussels, Belgium) at 60 mg/kg. After midline laparotomy, a tumor tissue cube of 1 – 2 mm^3 freshly harvested from a donor rat was implanted into the small incision made on the liver capsule [13]. The tumor growth was followed with MRI every 2 days, 1 week after the implantation until the tumor diameter reached 8–14 mm for therapy.

Antitumor drugs

CA4P (OxiGene; Watertown, Massachusetts, USA) was diluted in phosphate-buffered saline; ZD6126 (AstraZeneca, Cheshire, UK) was formulated in 20% of 5% sodium carbonate and 80% phosphate-buffered saline, yielding a clear solution at ca. pH 7.4 [14]. They were both intravenously injected at a clinically relevant dose of 10 mg/kg for the anticancer treatment to mimic the clinical scenario.

Experiment protocol

Thirty rats bearing tumor in the liver were randomly divided into the CA4P group ($n = 10$) with intravenous injection of CA4P at 10 mg/kg, ZD6126 group ($n = 10$) with ZD6126 at 10 mg/kg, or vehicle control ($n = 10$). All rats received a pretreatment baseline MRI. After the treatment with either VDA or vehicle, they underwent follow-up at 1 h, 6 h, 24 h, 48 h, and 120 h with MRI. Immediately after the last imaging session, the rats were killed for postmortem microangiography and histopathological verifications.

Magnetic resonance imaging

MRI was carried out with a clinical 1.5 T whole-body MR magnet (Symphony; Siemens, Erlangen, Germany) with a maximum gradient capability of 30 mT/m using a 4-channel phased array wrist coil (MRI Devices, Waukesha, Wisconsin, USA). The rat was gas anesthetized with 2% isoflurane in the mixture of 20% oxygen and 80% room air, through a mask connected by a tube to a Harvard Apparatus system (Holliston, Massachusetts, USA). The rat was placed in the supine position in a plastic holder with the penile vein cannulated for contrast agent and drug administration.

Sixteen axial images were acquired with a slice thickness of 2.0 mm and a gap of 0.4 mm for all the MRI sequences, including T2-weighted imaging (T2WI), T1-weighted imaging (T1WI), DWI, DCE-MRI, and contrast-enhanced T1WI (CE-T1WI). The imaging acquisition parameters are detailed in Table 1.

During the DCE-MRI, dotarem (Gadoterate Meglumine; Guerbet, Brussels, Belgium) was intravenously injected at 0.02 mmol/kg after a precontrast baseline of 30 measurements and the acquisition lasted until 100th measurement. Immediately after DCE-MRI, dotarem was intravenously injected again at 0.10 mmol/kg for acquiring CE-T1WI.

Table 1 Parameters for magnetic resonance imaging sequences

	T1WI	T2WI	DWI	DCE-MRI	CE-T1WI
Sequence type	TSE	TSE	EPI	T1-weighted GE	TSE
Repetition time/echo time (ms)	650/9.2	3810/100	1700/84	6.97/2.61	650/9.2
Flip angle (°)	90	90	90	10	90
Turbo factor	7	19	–	–	7
Field of view (mm^2)	70×140	70×140	82×140	81×130	70×140
Imaging acquisition matrix	128×256	128×256	91×192	96×192	128×256
In-plane resolution (mm^2)	0.55×0.55	0.55×0.55	0.90×0.73	0.84×0.68	0.55×0.55
Number of averages	4	3	6	1	4
Total acquisition time	1 min 42 s	1 min 25 s	4 min 57 s	6 min 10 s	1 min 42 s
Contrast agent (mmol/kg)	–	–	–	0.02	0.10
Diffusion gradients (s/mm^2)	–	–	0, 50, 100, 150, 200, 250, 300, 500, 750, 1000	–	–

CE-T1WI contrast-enhanced T1-weighted imaging; DWI, diffusion-weighted imaging; DCE-MRI, dynamic contrast-enhanced magnetic resonance imaging; EPI, echo-planar imaging; GE, gradient echo; T2WI, T2-weighted imaging; TSE turbo spin echo.

Ex-vivo digital microangiography

For the microangiography of tumor vasculature, barium sulfate suspension (Micropaque; Guerbet, Roissy, Cedex, France) was injected through the hepatic artery. The tumor-bearing liver was excised and radiographed with a digital mammographic unit (Mammomat Inspiration; Siemens, Erlangen, Germany) at 26 kV and 15 mA. Afterward, the liver was fixed in 10% formaldehyde.

Histopathology

The liver sections were embedded with paraffin and cut into 5 μm-thick slices, followed by hematoxylin–eosin staining for microscopic assessment for the presence and extent of viable tumor cells, necrosis, and tumor vasculature. The photomicrographs were further colocalized with the corresponding MR images.

Magnetic resonance imaging analyses

MRI analyses were all performed with the built-in software of the system (SyngoMR A30; Siemens, Erlangen, Germany), except DCE-MRI.

Tumor volume

On T2WI, tumor area was manually delineated with a freehand region of interest (ROI) on all tumor-containing images. The total tumor volume was calculated using the following equation:

$$\text{Tumor volume} = \sum \text{tumor area on each tumor-containing slice} \,(\text{slice thickness} + \text{gap}) \quad (1)$$

Tumor enhancement ratio

On T1WI and CE-T1WI, the whole tumor was delineated with ROI and the average signal intensity (SI) was generated from the voxels within the ROI. Tumor contrast enhancement at baseline and 1 h, 6 h, 24 h, 48 h, and 120 h posttreatment was compared using the following formula:

$$\text{Tumor enhancement ratio (ER)} = \left(SI_{\text{post-CE-T1}} - SI_{\text{post-T1}}\right) / \left(SI_{\text{pre-CE-T1}} - SI_{\text{pre-T1}}\right) \quad (2)$$

Where ER indicates the SI enhancement posttreatment relative to the baseline; $SI_{\text{post-T1}}$ and $SI_{\text{post-CE-T1}}$ denote the SI measured on posttreatment T1WI and CE-T1WI, respectively; and $SI_{\text{pre-T1}}$ and $SI_{\text{pre-CE-T1}}$ represent the SI on pretreatment T1WI and CE-T1WI, respectively. ER was calculated on the central tumor-containing slice. The percentile change in ER at different time points after treatment was defined by the following equation:

$$\left(ER_{\text{posttreatment}} - ER_{\text{baseline}}\right) / ER_{\text{baseline}} \times 100\,\% \quad (3)$$

Tumor necrosis ratio

Five days (120 h) after treatment, the volumes of intratumoral necrosis as the central nonenhancing mass within the tumor were obtained from the images of CE-T1WI immediately after contrast administration using an equation similar to that for tumor volume (1). The percentile change in necrosis ratio was defined as the volume of central necrosis over that of entire tumor.

Diffusion-weighted imaging

Apparent diffusion coefficient (ADC) map was calculated from DWI to quantify therapeutic effects by using the following widely applied monoexponential equation [15]

$$S_i = S_0 \exp\left(-b_i \,\text{ADC}\right) \quad (4)$$

where S_i is the SI measured on the ith b value image and b_i is the corresponding b value. S_0 is a variable that estimates the intrinsic SI (for $b = 0\,s/mm^2$). The percentile change in ADC at different time points after treatment was defined by the following equation:

$$\left(ADC_{\text{posttreatment}} - ADC_{\text{baseline}}\right) / ADC_{\text{baseline}} \times 100\,\% \quad (5)$$

Dynamic contrast-enhanced magnetic resonance imaging

The analysis of DCE-MRI was performed with NordicICE software (version 2.3.3; NordicNeuroLab, Bergen, Norway). As a low gadolinium dose was used, we could assume that there is a linear relation between the amount

of contrast agent in the tissue and the resultant difference in the relaxation time [16]. Global signal curve for the DCE-MRI was converted into percentile change in SI. Arterial input function was automatically detected with the cluster analysis. The map of K^{trans}, volume transfer constant per unit volume of tissue (unit/min), was generated by fitting the Tofts and Kermode model. The percentile change in K^{trans} at different time points after treatment was defined by the following equation:

$$\left(K^{trans}_{posttreatment} - K^{trans}_{baseline}\right) / K^{trans}_{baseline} \times 100\,\% \quad (6)$$

Statistical analysis

Statistical analysis was carried out with the Microsoft Office Excel 2007 and SPSS for Windows software package (version 16.0; SPSS, Chicago, Illinois, USA). In-vivo imaging biomarkers in the three groups were compared using multiple comparisons with the least significant difference test at different time points. Numerical data were reported as mean ± standard deviation, and a significant difference was concluded for a P value of less than 0.05.

Results

General conditions

All rats survived the entire experimental procedure including anesthesia, tumor implantation and growth, and multiple MRI sessions. The tumor model of liver was successfully established in all rats. They all tolerated well the intravenous administration of either CA4P or ZD6126 or the vehicles, without pallor, piloerection, restlessness, weakness, tremors, diarrhea, ascites, and loss of hair or appetite, suggesting the absence of detectable side effects.

In-vivo multiparametric imaging biomarkers

At baseline

Before treatment, all tumors were homogeneously hyperintense on T2WI, hypointense on T1WI, slightly hyperintense on ADC, and strongly enhanced on CE-T1WI (Figs 1, 2). The tumor volume, enhancement ratio, necrosis ratio, ADC, and K^{trans} did not show significant difference between the control and treated animals, nor showed statistical difference between different time points posttreatment in controls ($P > 0.05$; Table 2).

Fig. 1

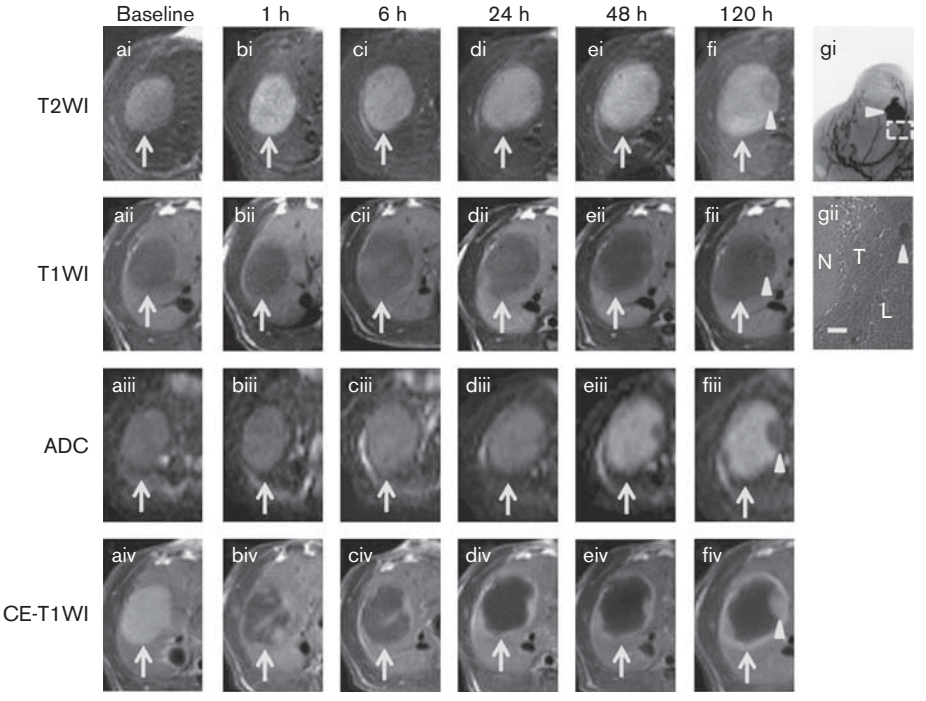

Findings in the combretastatin A4 phosphate (CA4P) group. At all time points, tumor was hyperintense on T2-weighted imaging (T2WI; ai – fi). When the treatment induced the formation of central necrosis, the viable tumor rim appeared relatively hypointense compared with necrotic center of hyperintensity from 24 to 120 h (di – fi). The tumor remained hypointense on T1-weighted imaging (T1WI) at all the time points (aii – fii). On apparent diffusion coefficient (ADC) map, the tumor appeared hyperintense at baseline (aiii); ADC decreased at 1 h (biii), but rebounded from 6 to 120 h (ciii – fiii). On contrast-enhanced (CE)-T1WI, the tumor was homogeneously enhanced at baseline (aiv), sporadically enhanced at 1 h (biv), and less enhanced at 6 h, suggesting that CA4P induced further vascular shutdown in tumor (civ). The tumor center remained unenhanced but with an enhanced rim from 24 to 120 h (div – fiv). On microangiography, tumor vessels largely diminished (gi). Microscopically (gii), the treatment-induced necrosis (N), peripheral viable tumor (T) with unaffected vessel (arrowhead), and normal liver (L) confirmed in-vivo findings (hematoxylin–eosin staining, × 100 original magnification, scale bar = 100 μm). Note the viable tumor nodule at the periphery on MRI (fi – iv, arrowheads) and corresponding blood pool on microangiography staining (gi, arrowhead).

Fig. 2

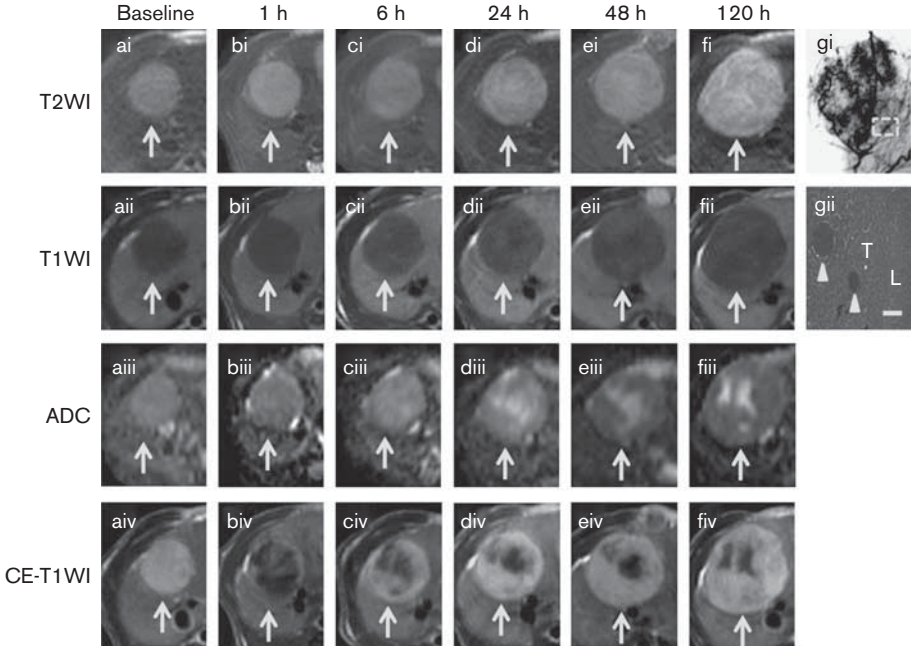

Findings in the ZD6126 group. At all time points, the tumor was hyperintense on T2-weighted imaging (T2WI; ai – fi) and hypointense on T1-weighted imaging (T1WI; aii – fii). On the apparent diffusion coefficient (ADC) map, the tumor appeared hyperintense at baseline (aiii); ADC decreased at 1 h (biii), but increased from 6 to 120 h (ciii – fiii). The irregular central necrosis was shown as hyperintensity compared with isointense viable tumor (diii – fiii). On contrast-enhanced (CE)-T1WI, the tumor was homogeneously enhanced at baseline (aiv), irregularly enhanced at 1 h (biv), and enhancement rim was gradually thicker from 6 to 12 h, indicating tumor recurrence (civ – fiv). There was abundant tumor staining on microangiography (gi). Photomicrograph (gii) showed viable tumor cells with greenish vessels (arrowheads) filled with barium sulfate (hematoxylin–eosin staining, × 100 original magnification, scale bar = 100 μm).

Table 2 The *P* values pretreatment and posttreatment among the three groups

	Baseline	1 h	6 h	24 h	48 h	120 h
Tumor volume						
CA4P vs. ZD6126	NS	NS	NS	NS	NS	<0.05
CA4P vs. control	NS	NS	NS	NS	<0.05	<0.05
ZD6126 vs. control	NS	NS	NS	NS	NS	NS
Enhancement ratio						
CA4P vs. ZD6126	NS	<0.05	<0.05	<0.05	<0.05	<0.05
CA4P vs. control	NS	<0.05	<0.05	<0.05	<0.05	<0.05
ZD6126 vs. control	NS	<0.05	<0.05	NS	NS	NS
ADC	NS					
CA4P vs. ZD6126	NS	NS	NS	<0.05	<0.05	<0.05
CA4P vs. control	NS	<0.05	<0.05	<0.05	<0.05	<0.05
ZD6126 vs. control	NS	<0.05	NS	<0.05	<0.05	NS
K^{trans}	NS					
CA4P vs. ZD6126	NS	NS	<0.05	<0.05	<0.05	<0.05
CA4P vs. control	NS	<0.05	<0.05	<0.05	<0.05	<0.05
ZD6126 vs. control	NS	<0.05	NS	NS	NS	NS

ADC, apparent diffusion coefficient; CA4P, combretastatin A4 phosphate; NS, not statistically significant ($P > 0.05$).

Tumor volume was $931.4 \pm 264.5\,mm^3$ in control, $945.5 \pm 251.4\,mm^3$ in CA4P, and $955.5 \pm 278.8\,mm^3$ in ZD6126 group, respectively ($P > 0.05$; Table 2). Enhancement ratio was 100% for all groups ($P > 0.05$; Table 2). ADC was $86.9 \pm 11.7 \times 10^{-3}\,mm^2/s$ in control, $85.2 \pm 10.8 \times 10^{-3}\,mm^2/sin$ CA4P, and $87.8 \pm 13.6 \times 10^{-3}\,mm^2/s$ in ZD6126 group, respectively ($P > 0.05$; Table 2). K^{trans} was 0.200 ± 0.086/min in control, 0.205 ± 0.073/min in CA4P, and 0.191 ± 0.064/min in the ZD6126 group, respectively ($P > 0.05$; Table 2). Necrosis ratio averaged $1.1 \pm 0.5\%$ in control, $0.8 \pm 0.4\%$ in CA4P, and $0.7 \pm 0.3\%$ in the ZD6126 group, respectively ($P > 0.05$; Table 2).

Comparison of therapeutic effects

Both CA4P and ZD6126 caused rapid vascular shutdown in tumors, induced tumor necrosis, and delayed the tumor growth compared with controls. CA4P appeared more effective than ZD6126 at every time point after treatment, and the most representative in-vivo images that are close to the mean values of imaging biomarkers are shown for the differential therapeutic effects (Figs 1–4). However, the tumor blood supply gradually rebounded after the VDA treatment of a single dose, which resulted in tumor recurrence at the periphery.

Tumor volume: CA4P and ZD6126 both delayed the tumor growth from 1 h to 120 h compared with controls. The tumor volume with CA4P was lower than with ZD6126 from 1 to 120 h with the statistical significance only at 120 h ($P < 0.05$; Figs 1, 2, 4a, Table 2). At 48 and 120 h, the tumor volume with CA4P was significantly lower than controls ($P < 0.05$; Figs 1, 4a, Table 2). ZD6126 also

Fig. 3

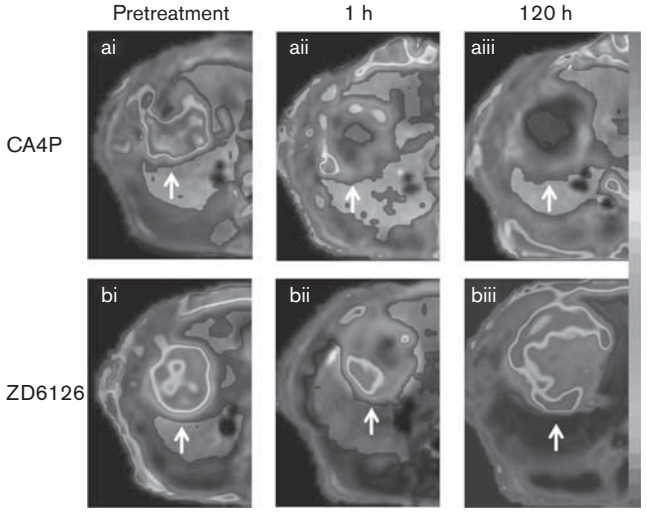

The dynamic changes in K^{trans}. The tumor (arrow) showed the abundant blood supply with high K^{trans} before treatment (ai, bi). At 1 h after vascular-disrupting agent (VDA) treatment, the vascular shutdown was indicated with low K^{trans} in the center, surrounded by the tumor residue at the periphery with moderate K^{trans} (aii, bii). At 120 h after the treatment, K^{trans} remained low with combretastatin A4 phosphate (CA4P; aiii), while the tumor relapsed upon the residue at the periphery with ZD6126, shown as rebounding K^{trans} (biii).

slowed down the tumor growth from 1 to 120 h compared with controls, but without significance ($P > 0.05$; Figs 2, 4a; Table 2).

Enhancement ratio: Both CA4P and ZD6126 caused an incomplete vascular shutdown as early as 1 h, shown as central irregular and thin peripheral enhancements ($P < 0.05$ for either VDA vs control; Figs 1biv, 2biv, 4b; Table 2). From 1 to 120 h, the enhancement ratio with CA4P remained lower than ZD6126 or its baseline value ($P < 0.05$ for CA4P vs. ZD6126 or control; Figs 1biv – fiv, 2biv–fiv, 4b; Table 2). The perfusion-inhibiting effect with CA4P reached its maximum at 6 h and only the enhanced ring still appeared on CE-T1WI (Fig. 1civ), whereas the blood perfusion began to rebound with ZD6126 at the same time point; this was reflected by the thicker enhancement ring of viable tumor on CE-T1WI ($P < 0.05$; Figs 2civ, 4b, Table 2). From 6 to 120 h, the viable ring with ZD6126 became even broader and more intensely enhanced; enhancement ratio continuously increased, exceeding the baseline value at 48 and 120 h ($P > 0.05$ vs. control; Figs 2civ – fiv, 4b; Table 2).

Apparent diffusion coefficient: Resulting from spontaneous necrosis, the ADC of control increased a little from baseline to 120 h (Fig. 4c; Table 2). ADC in the both treated groups significantly decreased compared with controls at 1 h, due to swelling of tumor cells and restricted water mobility in the extracellular space after vascular shutdown ($P < 0.05$ for either VDA vs. control; Figs 1biii, 2biii, 4c; Table 2). In treated groups, a continuous increase in ADC was observed from 1 to 120 h (Figs 1biii – fiii, 2biii – fiii, 4c), whereas the statistical significance between CA4P and ZD6126 was only reached at 24, 48, and 120 h ($P < 0.05$; Table 2). For CA4P, ADC was significantly higher than control from 24 to 120 h ($P < 0.05$; Figs 1diii – fiii, 4c; Table 2). However, with ZD6126, ADC was only significantly higher than control at 24 and 48 h ($P < 0.05$; Figs 2diii, eiii, 4c; Table 2). At 120 h, ADC with ZD6126 dropped again due to tumor relapse (Figs. 2fiii, 4c).

K^{trans}: At 1 h, K^{trans} significantly decreased in both treatment groups compared with control ($P < 0.05$; Figs. 3aii, bii, 4d; Table 2). At 6 h, there was a further drop in K^{trans} with CA4P and subsequent recovery to baseline value from 24 h, whereas the K^{trans} with ZD6126 started to recover from 6 h ($P < 0.05$; Fig. 4d). From 6 to 120 h, K^{trans} with CA4P stayed lower than ZD6126 or baseline value and showed a significant difference from ZD6126 ($P < 0.05$; Figs 3aiii, biii, 4d, Table 2). From 48 to 120 h, K^{trans} with ZD6126 was higher than control, sharing a similar trend with enhancement ratio (Fig. 4d).

Necrosis ratio: At 120 h, both VDAs induced a significantly higher necrosis ratio than controls with $3.1 \pm 2.3\%$ ($P < 0.05$ for either VDA vs control); $49.7 \pm 15.0\%$ with CA4P was significantly higher than $18.9 \pm 10.7\%$ with ZD6126 ($P < 0.05$; Figs. 1fiv, 2fiv; Table 2).

Ex-vivo findings

On microangiography, tumor staining with CA4P (Fig. 1gi) was obviously absent only with neoangiogenesis at the periphery, whereas there were abundant blood vessels due to tumor recurrence with ZD6126 (Fig. 2gi). On hematoxylin–eosin staining, tumor treated with CA4P showed extensive central necrosis with viable rim (Fig. 1gii) in comparison with hypervascular tumor of focal necrosis (uninvolved in the view) in ZD6126 group (Fig. 2gii).

Discussion

The differential therapeutic efficacy between CA4P and ZD6126

In this study, we could demonstrate that at a clinically relevant dose, both CA4P and ZD6126 caused selective vascular shutdown in tumor models of rat liver; CA4P was more potent than ZD6126 until 120 h after treatment. To our knowledge, it is the first time that such a comparative study between CA4P and ZD6126 was performed with in-vivo noninvasive multiparametric MRI biomarkers.

Several studies have shown that tumor blood supply is compromised within minutes after VDA treatment [17,18]. In this study, the vascular shutdown effect was detected with imaging biomarkers including enhancement ratio, K^{trans}, and ADC at 1 h in both treated

Fig. 4

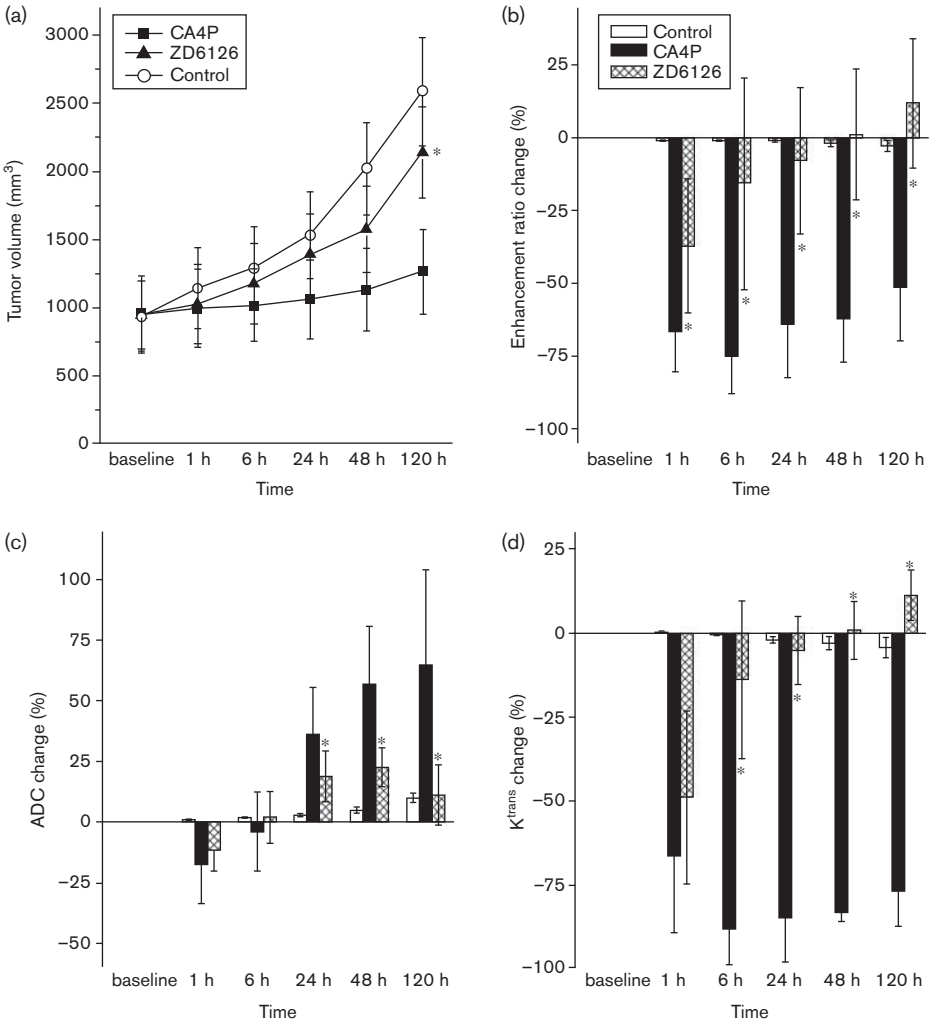

Quantification of magnetic resonance imaging (MRI) biomarkers before and after treatment. Line chart (a) compares tumor volumes at different time points in three groups. Tumors in treatment groups showed a delayed growth, with the tumor volume with combretastatin A4 phosphate (CA4P) being smaller than ZD6126 or control at every time point. Bar charts (b–d) show the percentile posttreatment change relative to baseline value. Enhancement ratio (b) decreased at 1 h after either vascular-disrupting agent (VDA) treatment, and further dropped with CA4P at 6 h, remaining low until 120 h, whereas the ratio started to return to baseline value with ZD6126 at 6 h and exceeded the baseline value from 48 to 120 h. Apparent diffusion coefficient (ADC; c) with VDAs dropped at 1 h and began to increase from 6 to 120 h. ADC with ZD6126 decreased again due to restricted diffusion by relapsing tumor cells at 120 h. K^{trans} (d) revealed the vascular shutdown with ZD6126 at 1 h and CA4P until 6 h, proceeded by the recovery of blood supply, a similar evolving trend with enhancement ratio. *$P<0.05$ for CA4P versus ZD6126.

groups, which was in line with previous studies. The degree of drop in blood supply with CA4P and ZD6126 reflected by K^{trans} and enhancement ratio was prominent at 1 h, and there was a further decrease with CA4P at 6 h, which caused the cytotoxic edema of tumor cells and decreased ADC. From 24 h on, the blood flow at the periphery of tumor started to regain and central necrosis developed, leading to elevated K^{trans}, enhancement ratio, and ADC value. Noteworthy, the vascular shutdown with ZD6126 was weaker than CA4P, and the blood supply was restored from 6 h. The recovery window of blood supply for CA4P and ZD6126 was consistent with other studies [19,20].

After a single dose of VDA, the inhibition of functional blood vessels can last some hours depending on the dose and tumor models. In this study, blood supply began to rebound for CA4P at 24 h, whereas for ZD6126 this occurred at 6 h. The evolution of CA4P effect was concordant with previous studies with the same dose [8,21]. Nevertheless, Bradley *et al.* [10] reported that in subcutaneous Hras5 tumors of athymic rats, ZD6126 at 5–10 mg/kg largely suppressed the blood supply by 55–77% at 24 h, which was more striking than our study with ZD6126 at the same time point. Although the therapeutic effects were only followed until 24 h in their experiment, it was clearly demonstrated that Hras5

tumor model in their study was more susceptible to ZD6126 treatment than rhabdomyosarcoma. In addition, the different immune statuses in athymic rats and rats with normal immune response in this experiment may contribute to the inconsistent therapeutic outcomes using the same dose of ZD6126. With regard to the clinical practice, the results of the rats with normal immune status may mirror the treatment efficacy in humans in a more accurate way [22].

Despite the massive central necrosis, a viable rim of tumor cells survives at the periphery, upon which tumor recurrence is unavoidable after single-dose VDA treatment [23–25]; this is because the tumor cells at the periphery can directly obtain nutrients and oxygen from neighboring normal tissues and engulfed normal vessels during the fast growth of tumor [26]. This explains why the tumor growth is only delayed and the tumor cannot be destroyed. In general, VDA treatment alone is not sufficient to eradicate the tumor mass, which limits the use of VDA as monotherapy and necessitates the combination therapy with other cytotoxic, hormonal or radiotherapy therapies to combat the treatment resistance [27–29].

The reason for the difference in efficacy between CA4P and ZD6126 at a clinically relevant dose on reducing blood supply in the same tumor model needs to be elucidated. CA4P is the prodrug of natural product, whereas ZD6126 is a synthetic compound. In plasma, ZD6126 has a longer half-life of about 1 h [30], whereas the half-life of CA4P is only 3.6 min [31]. CA4P and ZD6126 both bind to the colchicine-binding site on tubulin of cytoskeleton [32,33]. The mechanism of the variations observed in this study after CA4P or ZD6126 treatment may lie in the structural difference and the efficiency with which they damaged the tumor vessels by regulating the signaling pathways to disrupt the integrity of cytoskeleton [26,34].

Interestingly, the restored blood supply with ZD6126 at 48 and 120 h exceeded the pretreatment level, as shown with the enhancement ratio and K^{trans}. Statistical significance was not reached; this variation was within the 'noise' of the model system. Another possible reason may be the posttreatment change in phenotype of tumor. The hypoxia in tumor after VDA treatment may upregulate hypoxia-inducible factor 1α, stimulate the expression of angiogenic gene, increase the level of vascular endothelial growth factor, and enhance angiogenesis process. Therefore, neoangiogenesis is accelerated in the tumors after VDA treatment [35,36].

Both VDAs have a broad therapeutic window in rats, and in most studies a high dose of VDA was used in preclinical research and some promising results were observed. However, such hopeful outcomes in animals sometimes failed to translate into human trials; this is because VDAs are often more tolerated in animals than in humans, and higher dose than the MTD in humans is not feasible. In this study, both VDAs were used at a clinically relevant dose in tumors within deep-located visceral organs, which better mimics the clinical scenarios and may consequently mirror their outcomes in human patients in a more predictable way [22,37].

Multiparametric magnetic resonance imaging biomarkers in VDA treatment

Approved by World Health Organization, changes in tumor size/volume are the classical criteria for evaluating tumor response to chemotherapies [38,39]. However, such criteria may not precisely estimate the immediate vascular shutdown effects by VDAs with novel drug mechanism. As we can see in this study, both CA4P and ZD6126 slowed down the tumor growth, but the significance was only reached for CA4P compared with control at 48 and 120 h. ZD6126 also inhibited tumor growth, but there was no significance in tumor volume compared with control. This phenomenon challenges the traditional, morphologically based assessment criteria of tumor response [40].

The extensive clinical trials with VDAs have urged us to develop more timely and sensitive imaging biomarkers to monitor early cellular events after VDA treatment before the morphological change can be detected. The study of MRI biomarkers has demonstrated that the tumor microenvironment and hemodynamics are crucial for tumor initiation, progression, and metastasis. Multiparametric MRI biomarkers are able to noninvasively probe the early vascular properties in VDA treatment with qualitative and quantitative evaluation of morphological, functional, and metabolic/molecular changes [41,42]. Thus, MRI biomarkers play an imperative role in determining tumor response to various therapy strategies, which is important in the management of patients with cancer to improve the therapeutic index by allowing better individualization of treatment [43]. The incomplete tumoricidal efficacy with ZD6126 demonstrated by the multiparametric MRI biomarkers in this study may justify the cessation of clinical and commercial development of this VDA product [37].

Comprehensive MRI biomarkers have different potential in terms of morphological, physiological, and metabolic/molecular meanings. In this study, tumor volume, enhancement ratio, necrosis ratio, ADC, and K^{trans} were used to compare the different therapeutic efficacies between CA4P and ZD6126. Tumor volume alone has been proved to be insufficient to monitor the growth delay and the treatment effects may be underestimated until a significant change in morphology can be observed. Enhancement ratio only reflects the distribution of contrast agents in vascular space and extravascular extracellular space. Although it can be used to roughly assess the blood supply, the physiological relation is still

undefined with the transendothelial process. Necrosis ratio was calculated basis on perfusion deficit on CE-T1WI and provided the estimation of necrosis in the dynamic follow-up [44]. Necrosis ratio on CE-MRI has been shown to correlate with that on histopathology despite underestimation of true necrosis, resulting from the inward diffusion of MRI contrast agent from viable rim into necrotic center [37].

Probing water molecular diffusion with macromolecular and microstructural changes, DWI is easy to perform and free of contrast agent. DWI has increasingly been used as an imaging biomarker in assessment of the tumor treatment response due to its noninvasiveness and sensitivity [45,46]. ADC is quantified from DWI without the influence of magnetic field strength and T2 shine-through effect [46]. In this study, the ADC change due to the treatment was observed before the morphological response. After treatment, water diffusion was restricted first due to hypoxia and Na^+–K^+ pump failure in the cell memebrane as early as 1 h and began to be enhanced afterward due to necrosis formation. At 1 h, CA4P caused more severe cytotoxic edema and consequent lower ADC than ZD6126, which accounted for that at 6 h, ADC with ZD6126 had surpassed the baseline value, whereas CA4P was still lower thereof. In the ZD6126 group at 120 h, the central necrosis was largely replaced by the relapsing tumor cells, and the effect of necrosis on ADC was counteracted by tumor recurrence, leading to decreased ADC compared with 48 h.

Using exogenously administered MRI contrast agents, DCE-MRI produces time-series dynamic images and enables the analysis of contrast kinetics within a tumor, which appears to be most relevant to the alterations in blood supply in VDA therapy. T1-weighted DCE-MRI with the two-compartment pharmacokinetic model adopted in this study returned the physiological parameter K^{trans}, capillary permeability surface area product per unit volume of tissue [16,47]. K^{trans} reflects the trade-off between blood flow, the endothelial permeability, and the endothelial surface area. Before treatment, tumor vessels are highly permeable, and therefore blood flow dominates K^{trans}, meaning K^{trans} is more perfusion weighted. After the treatment, both blood flow and functional endothelial surface area are reduced; K^{trans} mirrors the combination of blood flow and permeability surface area product [48,49].

Study limitations

In this study, the imaging analyses of DWI and DCE-MRI were performed on the whole tumor. Owing to the treatment resistance, there was always a tumor residue at the periphery surrounding the necrotic center. Such heterogeneity of tumor response to VDAs was not analyzed on a pixel-by-pixel basis. Characterization of heterogeneous response in tumor may provide more predictable information for the prognosis [50,51]. In addition, perfused vascular volume markers such as Hoechst 33342 were not used in this experiment for more robust validation of in-vivo imaging data.

In conclusion, both CA4P and ZD6126 at a clinically relevant dose induced vascular shutdown in rhabdomyosarcoma of rat liver. CA4P was more effective than ZD6126 in sustaining tumor blood supply and delaying tumor growth in this tumor model. Multiparametric MRI biomarkers enabled the quantification of vascular shutdown, necrosis formation, and tumor recurrence after VDA treatment.

Acknowledgments

Supporting foundations: this study was partially supported by the grants awarded by FondsvoorWetenschappelijkOnderzoek-Vlaanderen (FWO Vlaanderen) Impulsfinanciering project (ZWAP/05/018), GeconcerteerdeOnderzoeksactie (GOA) of the Flemish Government, OT project (OT/06/70), the K.U. Leuven Molecular Small Animal Imaging Center MoSAIC (KUL EF/05/08), the Center of Excellence In vivo Molecular Imaging Research of KUL, and an EU project Asia-Link CfP 2006-EuropeAid/123738/C/ACT/Multi-Proposal No. 128-498/111.The contents of this paper are the sole responsibility of Leuven University, Belgium, and under no circumstances can be regarded as reflecting the position of the European Union.

Conflicts of interest

There are no conflicts of interest.

References

1 Denekamp J. Angiogenesis, neovascular proliferation and vascular pathophysiology as targets for cancer therapy. *Br J Radiol* 1993; **66**:181–196.
2 Tozer GM, Kanthou C, Baguley BC. Disrupting tumour blood vessels. *Nat Rev Cancer* 2005; **5**:423–435.
3 Heath VL, Bicknell R. Anticancer strategies involving the vasculature. *Nat Rev Clin Oncol* 2009; **6**:395–404.
4 Pettit GR, Singh SB, Hamel E, Lin CM, Alberts DS, Garcia-Kendall D. Isolation and structure of the strong cell growth and tubulin inhibitor combretastatin A-4. *Experientia* 1989; **45**:209–211.
5 Davis PD, Dougherty GJ, Blakey DC, Galbraith SM, Tozer GM, Holder AL, *et al*. ZD6126: a novel vascular-targeting agent that causes selective destruction of tumor vasculature. *Cancer Res* 2002; **62**:7247–7253.
6 Hinnen P, Eskens FA. Vascular disrupting agents in clinical development. *Br J Cancer* 2007; **96**:1159–1165.
7 Robinson SP, McIntyre DJ, Checkley D, Tessier JJ, Howe FA, Griffiths JR, *et al*. Tumour dose response to the antivascular agent ZD6126 assessed by magnetic resonance imaging. *Br J Cancer* 2003; **88**:1592–1597.
8 Siemann DW, Chaplin DJ, Walicke PA. A review and update of the current status of the vasculature-disabling agent combretastatin-A4 phosphate (CA4P). *Expert Opin Investig Drugs* 2009; **18**:189–197.
9 Prise VE, Honess DJ, Stratford MR, Wilson J, Tozer GM. The vascular response of tumor and normal tissues in the rat to the vascular targeting agent, combretastatin A-4-phosphate, at clinically relevant doses. *Int J Oncol* 2002; **21**:717–726.
10 Bradley DP, Tessier JJ, Ashton SE, Waterton JC, Wilson Z, Worthington PL, *et al*. Correlation of MRI biomarkers with tumor necrosis in Hras5 tumor xenograft in athymic rats. *Neoplasia* 2007; **9**:382–391.
11 Breidahl T, Nielsen FU, Stodkilde-Jorgensen H, Maxwell RJ, Horsman MR. The effects of the vascular disrupting agents combretastatin A-4 disodium phosphate, 5,6-dimethylxanthenone-4-acetic acid and ZD6126 in a murine

tumour: a comparative assessment using MRI and MRS. *Acta Oncol* 2006; **45**:306–316.
12 Hermens AF, Barendsen GW. Cellular proliferation patterns in an experimental rhabdomyosarcoma in the rat. *Eur J Cancer* 1967; **3**:361–369.
13 Chen F, Sun X, De Keyzer F, Yu J, Peeters R, Coudyzer W, *et al*. Liver tumor model with implanted rhabdomyosarcoma in rats: MR imaging, microangiography, and histopathologic analysis. *Radiology* 2006; **239**:554–562.
14 Madhu B, Waterton JC, Griffiths JR, Ryan AJ, Robinson SP. The response of RIF-1 fibrosarcomas to the vascular-disrupting agent ZD6126 assessed by in-vivo and ex-vivo 1H magnetic resonance spectroscopy. *Neoplasia* 2006; **8**:560–567.
15 Sun X, Wang H, Chen F, De Keyzer F, Yu J, Jiang Y, *et al*. Diffusion-weighted MRI of hepatic tumor in rats: comparison between *in vivo* and postmortem imaging acquisitions. *J Magn Reson Imaging* 2009; **29**:621–628.
16 Tofts PS, Berkowitz BA. Rapid measurement of capillary permeability using the early part of the dynamic Gd-DTPA MRI enhancement curve. *J Magn Reson B* 1993; **102**:129–136.
17 Ching LM, Zwain S, Baguley BC. Relationship between tumour endothelial cell apoptosis and tumour blood flow shutdown following treatment with the antivascular agent DMXAA in mice. *Br J Cancer* 2004; **90**:906–910.
18 Seshadri M, Spernyak JA, Maiery PG, Cheney RT, Mazurchuk R, Bellnier DA. Visualizing the acute effects of vascular-targeted therapy *in vivo* using intravital microscopy and magnetic resonance imaging: correlation with endothelial apoptosis, cytokine induction, and treatment outcome. *Neoplasia* 2007; **9**:128–135.
19 Horsman MR, Murata R. Vascular targeting effects of ZD6126 in a C3H mouse mammary carcinoma and the enhancement of radiation response. *Int J Radiat Oncol Biol Phys* 2003; **57**:1047–1055.
20 Murata R, Overgaard J, Horsman MR. Comparative effects of combretastatin A-4 disodium phosphate and 5,6-dimethylxanthenone-4-acetic acid on blood perfusion in a murine tumour and normal tissues. *Int J Radiat Biol* 2001; **77**:195–204.
21 Wang H, Sun X, Chen F, De Keyzer F, Yu J, Landuyt W, *et al*. Treatment of rodent liver tumor with combretastatin A4 phosphate: noninvasive therapeutic evaluation using multiparametric magnetic resonance imaging in correlation with microangiography and histology. *Invest Radiol* 2009; **44**:44–53.
22 Ni Y, Wang H, Chen F, Li J, DeKeyzer F, Feng Y, *et al*. Tumor models and specific contrast agents for small animal imaging in oncology. *Methods* 2009; **48**:125–138.
23 Chen G, Horsman MR, Pedersen M, Pang Q, Stødkilde-Jørgensen H. The effect of combretastatin A4 disodium phosphate and 5,6-dimethylxanthenone-4-acetic acid on water diffusion and blood perfusion in tumours. *Acta Oncol* 2008; **47**:1071–1076.
24 Delmonte A, Sessa C. AVE8062: a new combretastatin derivative vascular disrupting agent. *Expert Opin Investig Drugs* 2009; **18**:1541–1548.
25 Sheng Y, Hua J, Pinney KG, Garner CM, Kane RR, Prezioso JA, *et al*. Combretastatin family member OXI4503 induces tumor vascular collapse through the induction of endothelial apoptosis. *Int J Cancer* 2004; **111**:604–610.
26 Kanthou C, Tozer GM. Microtubule depolymerizing vascular disrupting agents: novel therapeutic agents for oncology and other pathologies. *Int J Exp Pathol* 2009; **90**:284–294.
27 Siemann DW, Shi W. Dual targeting of tumor vasculature: combining avastin and vascular disrupting agents (CA4P or OXi4503). *Anticancer Res* 2008; **28**:2027–2031.
28 Landuyt W, Ahmed B, Nuyts S, Theys J, Op de Beeck M, Rijnders A, *et al*. In-vivo antitumor effect of vascular targeting combined with either ionizing radiation or anti-angiogenesis treatment. *Int J Radiat Oncol Biol Phys* 2001; **49**:443–450.
29 Murata R, Overgaard J, Horsman MR. Combretastatin A-4 disodium phosphate: a vascular targeting agent that improves that improves the anti-tumor effects of hyperthermia, radiation, and mild thermoradiotherapy. *Int J Radiat Oncol Biol Phys* 2001; **51**:1018–1024.
30 Blakey DC, Ashton SE, Westwood FR, Walker M, Ryan AJ. ZD6126: a novel small molecule vascular targeting agent. *Int J Radiat Oncol Biol Phys* 2002; **54**:1497–1502.
31 Siemann DW. The unique characteristics of tumor vasculature and preclinical evidence for its selective disruption by tumor-vascular disrupting agents. *Cancer Treat Rev* 2011; **37**:63–74.
32 Micheletti G, Poli M, Borsotti P, Martinelli M, Imberti B, Taraboletti G, *et al*. Vascular-targeting activity of ZD6126, a novel tubulin-binding agent. *Cancer Res* 2003; **63**:1534–1537.
33 Lippert JW 3rd. Vascular disrupting agents. *Bioorg Med Chem* 2007; **15**:605–615.
34 Tozer GM, Kanthou C, Lewis G, Prise C, Vojnovic B, Hill SA. Tumour vascular disrupting agents: combating treatment resistance. *Br J Radiol* 2008; **81**:S12–S20.
35 Sheng Y, Hua J, Pinney KG, Garner CM, Kane RR, Prezioso JA, *et al*. Combretastatin family member OXI4503 induces tumor vascular collapse through the induction of endothelial apoptosis. *Int J Cancer* 2004; **111**:604–610.
36 Dachs GU, Steele AJ, Coralli C, Kanthou C, Brooks AC, Gunningham SP, *et al*. Anti-vascular agent combretastatin A-4-P modulates hypoxia inducible factor-1 and gene expression. *BMC Cancer* 2006; **6**:280.
37 Wang H, Li J, Chen F, De Keyzer F, Yu J, Feng Y, *et al*. Morphological, functional and metabolic imaging biomarkers: assessment of vascular-disrupting effect on rodent liver tumours. *Eur Radiol* 2010; **20**:2013–2026.
38 Miller AB, Hoogstraten B, Staquet M, Winkler A. Reporting results of cancer treatment. *Cancer* 1981; **47**:207–214.
39 Therasse P, Arbuck SG, Eisenhauer EA, Wanders J, Kaplan RS, Rubinstein L, *et al*. New guidelines to evaluate the response to treatment in solid tumors. European Organization for Research and Treatment of Cancer, National Cancer Institute of the United States, National Cancer Institute of Canada. *J Natl Cancer Inst* 2000; **92**:205–216.
40 Padhani AR, Miles KA. Multiparametric imaging of tumor response to therapy. *Radiology* 2010; **256**:348–364.
41 Harry VN, Semple SI, Parkin DE, Gilbert FJ. Use of new imaging techniques to predict tumour response to therapy. *Lancet Oncol* 2010; **11**:92–102.
42 Tozer GM. Measuring tumour vascular response to antivascular and antiangiogenic drugs. *Br J Radiol* 2003; **76**:S23–S35.
43 Jordan BF, Gallez B. Surrogate MR markers of response to chemo- or radiotherapy in association with co-treatments: a retrospective analysis of multi-modal studies. *Contrast Media Mol Imaging* 2010; **5**:323–332.
44 Lang P, Wendland MF, Saeed M, Gindele A, Rosenau W, Mathur A, *et al*. Osteogenic sarcoma: noninvasive in vivo assessment of tumor necrosis with diffusion-weighted MR imaging. *Radiology* 1998; **206**:227–235.
45 Thoeny HC, Ross BD. Predicting and monitoring cancer treatment response with diffusion-weighted MRI. *J Magn Reson Imaging* 2010; **32**:2–16.
46 Padhani AR, Liu G, Mu-Koh D, Chenevert TL, Thoeny HC, Takahara T, *et al*. Diffusion-weighted magnetic resonance imaging as a cancer biomarker: consensus and recommendations. *Neoplasia* 2009; **11**:102–125.
47 Tofts PS. Modeling tracer kinetics in dynamic Gd-DTPA MR imaging. *J Magn Reson Imaging* 1997; **7**:91–101.
48 Tofts PS, Brix G, Buckley DL, Evelhoch JL, Henderson E, Knopp MV, *et al*. Estimating kinetic parameters from dynamic contrast-enhanced T(1)-weighted MRI of a diffusable tracer: standardized quantities and symbols. *J Magn Reson Imaging* 1999; **10**:223–232.
49 Collins DJ, Padhani AR. Dynamic magnetic resonance imaging of tumor perfusion: approaches and biomedical challenges. *IEEE Eng Med Biol Mag* 2004; **23**:65–83.
50 Jackson A, O'Connor JP, Parker GJ, Jayson GC. Imaging tumor vascular heterogeneity and angiogenesis using dynamic contrast-enhanced magnetic resonance imaging. *Clin Cancer Res* 2007; **13**:3449–3459.
51 Koh DM, Blackledge M, Collins DJ, Padhani AR, Wallace T, Wilton B, *et al*. Reproducibility and changes in the apparent diffusion coefficients of solid tumours treated with combretastatin A4 phosphate and bevacizumab in a two-centre phase I clinical trial. *Eur Radiol* 2009; **19**: 2728–2738.